10-6-2020

Brown adipose expansion and remission of glycemic dysfunction in obese SM/J mice

Caryn Carson

Juan F Macias-Velasco

Subhadra Gunawardana

Mario A Miranda

Sakura Oyama

See next page for additional authors

Authors

Caryn Carson, Juan F Macias-Velasco, Subhadra Gunawardana, Mario A Miranda, Sakura Oyama, Celine L St Pierre, Heather Schmidt, Jessica P Wayhart, and Heather A Lawson

Cell Reports

Brown Adipose Expansion and Remission of Glycemic Dysfunction in Obese SM/J Mice

Graphical Abstract

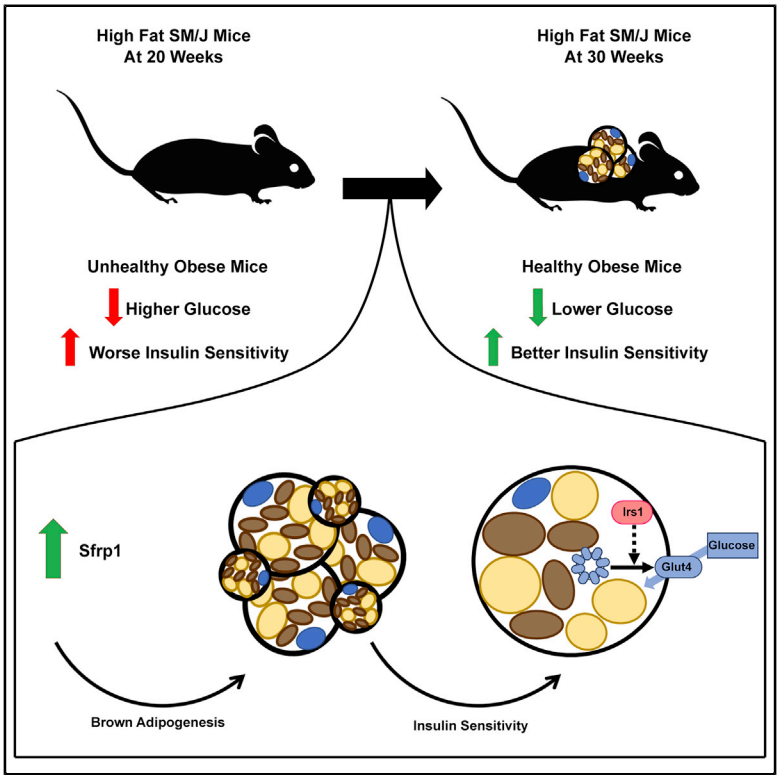

Highlights

- High-fat-fed SM/J mice develop disproportionate expansion of brown adipose
- The increased brown adipose improves insulin-stimulated glucose uptake
- Expanded brown adipose has a healthier transcriptional profile and lower inflammation
- *Sfrp1* expression correlates with brown adipogenesis and glucose homeostasis

Authors

Caryn Carson, Juan F. Macias-Velasco, Subhadra Gunawardana, ..., Heather Schmidt, Jessica P. Wayhart, Heather A. Lawson

Correspondence

lawson@wustl.edu

In Brief

Carson et al. characterize the spontaneous development of a disproportionate expansion of brown adipose tissue in obese SM/J mice. They find the mice with increased brown adipose tissue have improved glucose tolerance and insulin sensitivity without weight loss, and identify the cytokine Sfrp1 as a likely cause of brown adipogenesis.

Carson et al., 2020, Cell Reports *33*, 108237
October 6, 2020
https://doi.org/10.1016/j.celrep.2020.108237

Cell Reports

CellPress
OPEN ACCESS

Report

Brown Adipose Expansion and Remission of Glycemic Dysfunction in Obese SM/J Mice

Caryn Carson,[1] Juan F. Macias-Velasco,[1] Subhadra Gunawardana,[2] Mario A. Miranda,[1] Sakura Oyama,[1] Celine L. St. Pierre,[1] Heather Schmidt,[1] Jessica P. Wayhart,[1] and Heather A. Lawson[1,3,*]

[1]Department of Genetics, Washington University School of Medicine, 660 South Euclid Ave., Saint Louis, MO 63108, USA

[2]Department of Cell Biology and Physiology, Washington University School of Medicine, 660 South Euclid Ave., Saint Louis, MO 63108, USA

[3]Lead Contact

*Correspondence: lawson@wustl.edu

https://doi.org/10.1016/j.celrep.2020.108237

SUMMARY

We leverage the SM/J mouse to understand glycemic control in obesity. High-fat-fed SM/J mice initially develop poor glucose homeostasis relative to controls. Strikingly, their glycemic dysfunction resolves by 30 weeks of age despite persistent obesity. The mice dramatically expand their brown adipose depots as they resolve glycemic dysfunction. This occurs naturally and spontaneously on a high-fat diet, with no temperature or genetic manipulation. Removal of the brown adipose depot impairs insulin sensitivity, indicating that the expanded tissue is functioning as an insulin-stimulated glucose sink. We describe morphological, physiological, and transcriptomic changes that occur during the brown adipose expansion and remission of glycemic dysfunction, and focus on Sfrp1 (secreted frizzled-related protein 1) as a compelling candidate that may underlie this phenomenon. Understanding how the expanded brown adipose contributes to glycemic control in SM/J mice will open the door for innovative therapies aimed at improving metabolic complications in obesity.

INTRODUCTION

An estimated 10%–30% of obese individuals maintain glycemic control, and some longitudinal studies suggest their risk of developing type II diabetes is no greater than matched lean individuals (Meigs et al., 2006). No causative factors underlying glycemic control in obesity have been discovered; however, the strongest predictors of impaired glycemic control in obesity are increased visceral fat mass and adipose tissue dysfunction (Goossens, 2017; Klöting et al., 2010). Thus, research efforts have focused on understanding the genetic and physiological mechanisms of action of adipose. Recent research reveals that brown adipose activity is associated with anti-diabetic properties. Cold exposure in both obese and lean individuals causes increased uptake of fatty acids and glucose into brown adipose tissue (Saito et al., 2009). Further, increased brown adipose activity has been shown to improve glucose homeostasis and insulin sensitivity in adults (Chondronikola et al., 2014). Transplantation of brown adipose tissue into mouse models of diabetes greatly improves glucose parameters, including fasting glucose levels and response to a glucose challenge (Gunawardana and Piston, 2012). Although there are a variety of obese and diabetic mouse models, there are no mouse models for understanding the relationship between brown adipose and glycemic control in obesity.

The SM/J inbred mouse strain has long been used for studying interactions between diet and metabolism, and more recently has started to help uncover the genetic architecture underlying diet-induced obesity and glucose homeostasis. It has previously been shown that fed a high-fat diet, SM/J mice display many of the characteristics of a diabetic-obese mouse: obesity, hyperglycemia, and glucose intolerance at 20 weeks of age (Cheverud et al., 2011; Ehrich et al., 2003; Lawson et al., 2010, 2011). We discovered that SM/J mice undergo a remarkable transformation between 20 and 30 weeks of age. Despite persistence of the obese state, these mice enter into diabetic remission: returning to normoglycemia and reestablishing glucose tolerance and improving insulin sensitivity. Contemporary with this remission of glycemic parameters is a dramatic expansion of the intrascapular brown adipose depot. Our results strongly suggest that SM/J's brown adipose contributes to their diabetic remission through non-thermogenic mechanisms, and we focus on the cytokine *Secreted Frizzled-Related Protein 1* (SFRP1) as a compelling candidate that may underlie this remarkable phenomenon. This study describes the morphological, physiological, and transcriptomic changes that occur during this transition, and establishes the SM/J mouse as a unique model for understanding the relationship between brown adipose and glycemic control in obesity. Understanding this relationship in a genetic model of glycemic resolution will set the stage for identifying novel, potentially therapeutic targets for the improvement of glycemic control.

RESULTS

SM/J Mice Improve Glucose Parameters without Weight Loss

When fed a high-fat diet (Table S1) from 3 weeks of age, SM/J mice develop obesity, hyperglycemia, and impaired glucose tolerance by 20 weeks (Ehrich et al., 2003). By 30 weeks, despite

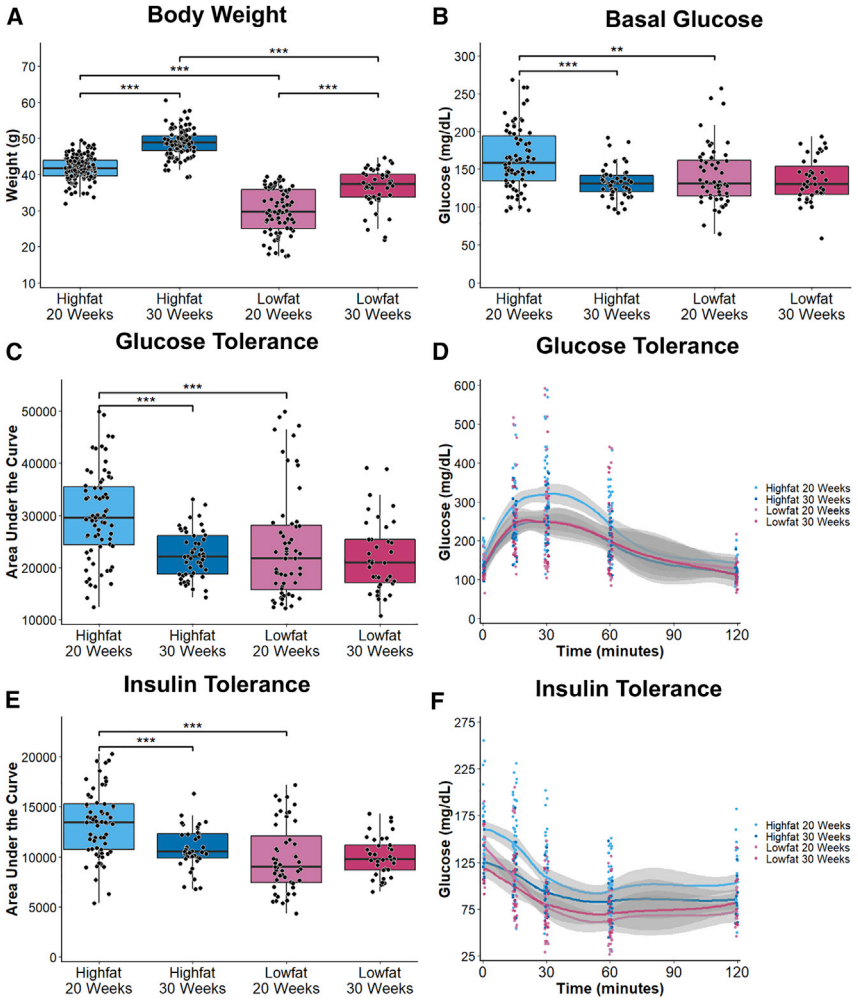

Figure 1. Obese SM/J Mice Improve Glucose Parameters between 20 and 30 Weeks of Age

(A) High-fat-fed mice weigh significantly more than low-fat-fed mice, and SM/J mice gain weight between 20 and 30 weeks of age on both diets; n = 140, 106, 78, and 48 mice in high-fat-fed 20, high-fat-fed 30, low-fat-fed 20, and low-fat-fed 30 cohorts.

(B) 30-week-old high-fat-fed mice have significantly lower fasting glucose levels than at 20 weeks.

(C and D) 30-week-old high-fat-fed mice have improved glucose tolerance relative to 20 weeks.

(E and F) Lower fasting glucose and improved glucose tolerance correspond with improved insulin sensitivity.

Equal numbers of males and females are represented; n = 39–49 mice per 30-week cohort; n = 51–71 mice per 20-week cohort. The boxplots display median, 1st and 3rd quartiles, and 1.5 × interquartile range for each cohort. Individual data points are also represented. *p < 0.05, **p < 0.01, ***p < 0.001. See also Figure S1.

the persistence of obesity, high-fat-fed SM/J mice resolve their hyperglycemia and impaired glucose tolerance to levels indistinguishable from low-fat-fed controls (Figures 1A–1D). Thirty-week high-fat-fed SM/J mice have dramatically increased serum and pancreatic insulin levels compared with 20-week animals (Miranda et al., 2020), and insulin sensitivity improves along with improved glycemic parameters (Figures 1E and 1F). Notably, metabolic hormones, such as adiponectin, glucagon, IGF1, and leptin, do not show any changes in circulating levels between 20 and 30 weeks (Figures S1A–S1D). Further, the changes in glucose phenotypes are not transient effects; rather, high-fat-fed animals maintain improved basal glucose, glucose tolerance, and insulin tolerance as they age (Figures S1E–S1I).

High-fat-fed C57BL/6J mice also show a reduction in fasting glucose that is accompanied by increased insulin with age (Winzell and Ahrén, 2004). In contrast with SM/J, the difference in circulating glucose between the high-fat- and low-fat-fed C57BL/6J mice remains significantly different over time. Moreover, high-fat-fed C57BL/6J mice show marked glucose intolerance that does not resolve with age. We observe a similar trend in the LG/J strain of mice, where high-fat-fed animals maintain higher fasting glucose levels and impaired glucose tolerance relative to low-fat-fed controls as they age (Figures S1J and S1L–S1P). The unique remission of hyperglycemia and improved glucose tolerance observed in the high-fat-fed SM/J strain indicate a genetic basis.

High-Fat-Fed SM/J Mice Expand Their Interscapular Brown Adipose Tissue Depots

Contemporary with the resolution of glycemic parameters, high-fat-fed SM/J mice dramatically expand their intrascapular brown adipose depots, which is not seen in low-fat-fed control mice (Figures 2A–2C). This has never been described in another mouse strain, and we do not observe the phenomenon in the LG/J strain of mice on the same diets at any age (Figure S1K). To understand whether the tissue mass expansion is due to increased size of individual cells or to increased number of total cells, we quantified adipocyte cell size and the mitotic index. There are no significant differences in average cell size in high-fat-fed mice between 20 and 30 weeks or relative to low-fat-fed controls (Figure S2A). Mice on both diets undergo altered adipocyte area profiles between 20 and 30 weeks of age; however, the low-fat tissue develops a profile significantly trending toward larger adipocytes at 30 weeks ($p = 6.4e^{-7}$), whereas the high-fat tissue develops a profile significantly trending toward smaller adipocytes at 30 weeks ($p = 2.2e^{-16}$) (Figures 2D and 2E). This suggests that the expansion of the brown adipose depot in high-fat-fed mice is not the result of increased lipid uptake into already existing adipocytes. Quantification of brown adipose cells stained positive for the mitotic marker phosphohistone H3 showed a trend toward a higher mitotic index in the brown adipose of high-fat-fed animals (Figure S2B), suggesting that the increased mass may be caused by an increased number of cells.

Because obesity has been associated with structural and functional "whitening" of brown adipose depots in rodents

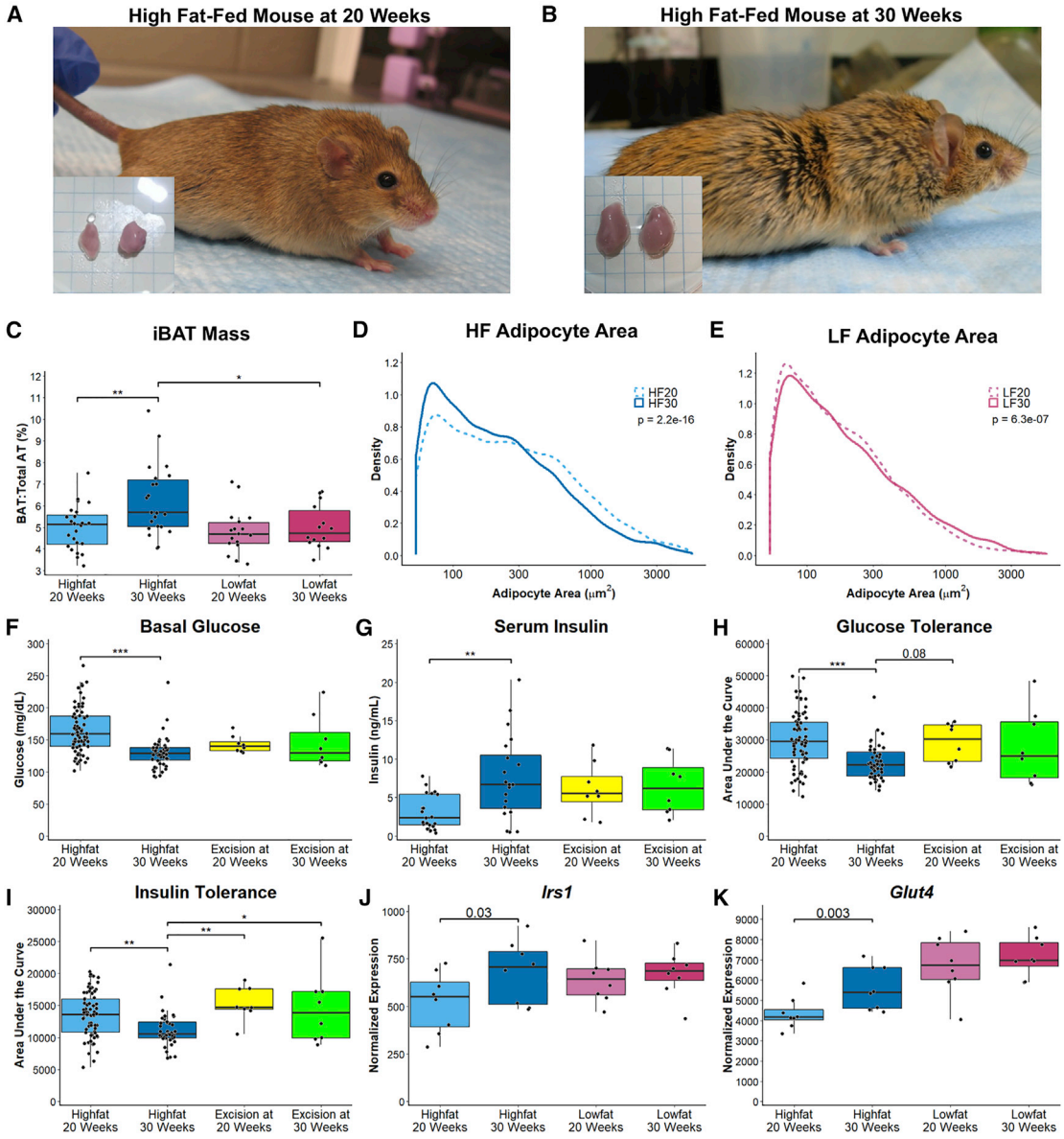

Figure 2. Brown Adipose Expansion in 30-Week-Old High-Fat-Fed SM/J Mice Is Required for Improved Insulin Tolerance

(A and B) Representative pictures of (A) 20- and (B) 30-week-old high-fat-fed female mice with insets showing larger brown adipose lobes in 30-week animals.

(C) Quantification of interscapular brown adipose depot as a proportion of total fat mass; n = 16–25 mice per cohort.

(D and E) Cell area density graphs for high-fat- and low-fat-fed cohorts. Data are plotted on a log10 scale for visualization; n = 4 mice per cohort.

(F–H) Fasting glucose (F) and insulin (G) and glucose (H) tolerance were not significantly altered by removal of the brown adipose depot before (20-week excision) or after (30-week excision) expansion.

(I) Insulin tolerance was significantly worse after brown adipose tissue (BAT) ablation; n = 8 mice per excision cohort.

(J and K) Expression of (J) *Irs1* and (K) *Glut4* increases significantly in expanded brown adipose depot; n = 8 mice per cohort.

Equal numbers of males and females are represented. The boxplots display median, 1st and 3rd quartiles, and 1.5 × interquartile range for each cohort. Line graphs were generated using loess regression and smoothing. Individual data points are also represented. *p < 0.05, **p < 0.01, ***p < 0.001. See also Figure S2.

(Lapa et al., 2017; Roberts-Toler et al., 2015; Shimizu and Walsh, 2015; Shimizu et al., 2014), we confirmed that the tissue expansion in SM/J mice has the expected properties of brown fat. Histological analysis of the fat depot taken from high-fat-fed SM/J mice at 30 weeks of age confirms the adipocytes in this expansion are brown adipocytes, with small multilocular lipid droplets and high UCP1 staining (Figures S2C–S2J). Expression of canonical brown adipose genes (*Ucp1*, *Cidea*, *Eva1*, *Prdm16*, *Pgc1a*) does not change between 20 and 30 weeks (Figures S2L–S2P), nor is there any evidence of a general "beiging" phenomenon in white adipose tissue (Wu et al., 2012). There is no significant difference in brown adipose tissue mitochondrial

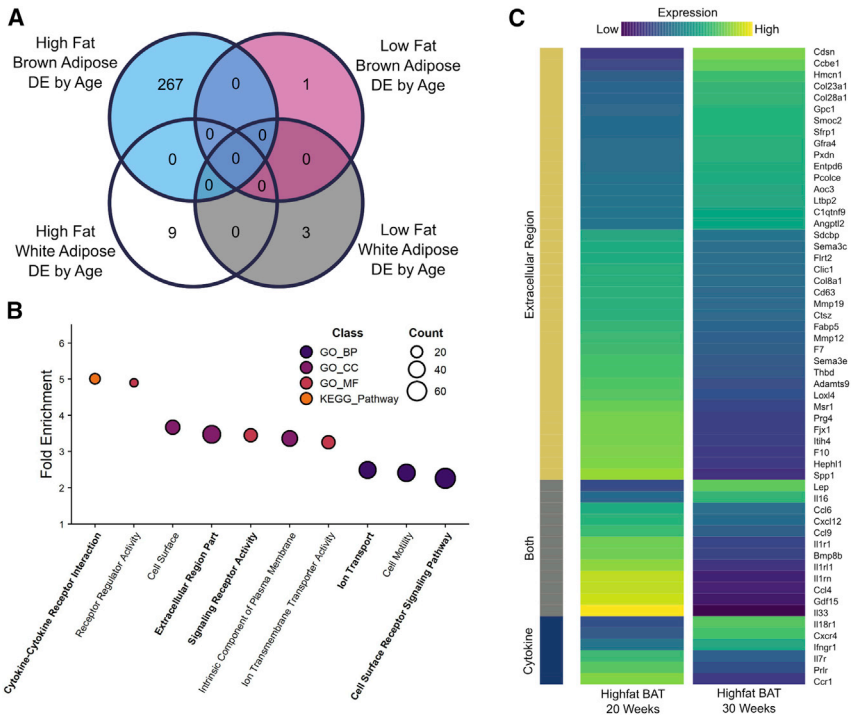

Figure 3. High-Fat-Fed SM/J Mice Have Unique Brown Adipose Differential Expression between 20 and 30 Weeks of Age

(A) Venn diagram illustrating the number of genes differentially expressed between high- and low-fat-fed 20- and 30-week-old SM/J interscapular brown or reproductive white adipose tissues.

(B) Terms enriched in genes differentially expressed by age in high-fat SM/J brown adipose colored by class: Gene Ontology Biological Process (GO_BP), Cellular Component (GO_CC), Molecular Function (GO_MF), and Kyoto Encyclopedia of Genes and Genomes (KEGG) pathway.

(C) Heatmap of differentially expressed brown adipose tissue genes belonging to cytokine, extracellular matrix, or both gene ontologies.

See also Tables S2 and S3.

content (Figure S2K), core body temperature, or circulating free fatty acids between high- and low-fat-fed cohorts or between 20 and 30 weeks of age (Figures S2U and S2V). Additionally, although there are diet-dependent differences in the catecholamines norepinephrine and epinephrine, which activate UCP1-mediated leak respiration and non-shivering thermogenesis, there is no change in levels between ages in the high-fat-fed mice (Figures S2W and S2X). Thus, the interscapular adipose depot in high-fat-fed SM/J mice maintains a brown adipose identity after expansion that is not dependent on whole-animal beiging and is also not associated with altered thermogenesis.

Expanded Brown Adipose Tissue Serves as an Insulin-Stimulated Glucose Sink

If the brown adipose expansion is directly related to the glycemic resolution of the high-fat-fed SM/J mice, preventing or removing that expansion should revert their glucose parameters to an unhealthy state. To test these predictions, we removed the interscapular brown adipose depots from hyperglycemic 20-week-old and normoglycemic 30-week-old mice. Interestingly, removal of the brown adipose depot at 20 weeks does not affect serum glucose or insulin levels, or the glucose tolerance of the animals, indicating that the expanded brown adipose is downstream of the primary signal (Figures 2F–2H) (Miranda et al., 2020). However, removal of the brown adipose depot before expansion prevents the natural improvement in insulin tolerance, and removal of the expanded tissue at 30 weeks results in a reversion to 20-week-old measurements (Figure 2I). These results strongly suggest that the expanding brown adipose tissue of obese SM/J mice serves as an insulin-stimulated glucose sink. This is supported by increased expression of both *Irs1* and *Glut4* (Figures 2J and 2K), key members of the insulin-stimulated glucose pathway (Pessin and Saltiel, 2000).

RNA Sequencing Reveals Enrichment of Differentially Expressed Cytokines and Genes Affecting Extracellular Matrix

Because the brown adipose tissue expansion is unique to high-fat-fed SM/J mice, we anticipated that there would be corresponding unique transcriptomic changes in the brown adipose. Indeed, we identified 267 genes whose expression significantly and uniquely changes between 20 and 30 weeks of age in high-fat-fed SM/J brown adipose tissue (at a 5% false discovery rate [FDR], out of 13,253 total genes expressed; Table S2). These expression changes occur when the mice resolve their glycemic dysfunction and expand their brown adipose depots. These genes are not differentially expressed in white adipose tissue taken from the same animals or in low-fat-fed SM/J controls (Figure 3A). Additionally, they are not differentially expressed in the LG/J strain of mouse, once again underscoring the genetic basis of the phenomenon (Table S3).

Over-representation analysis indicates these genes are enriched for those involved in cytokine-cytokine receptor interactions ($p = 3.23e^{-6}$), signaling receptor activity ($p = 5.70e^{-6}$), cell surface receptor signaling ($p = 2.04e^{-7}$), and extracellular matrix (ECM) components ($p = 7.93e^{-13}$) (Figure 3B). Several genes belonging to these biological categories have evidence for their involvement in glucose homeostasis and change expression in a direction that is associated with improved metabolic health in high-fat-fed SM/J mice between 20 and 30 weeks of age (Figure 3C; Table S2). These are intriguing results because brown adipose has been identified as a source of cytokines that influences glucose homeostasis, and extracellular matrix changes are essential for tissue expansion, cellular signaling, and regulation of growth factor bioavailability (Lin and Farmer, 2016; Wang et al., 2015). However, extreme changes in ECM protein levels are associated with adipose dysfunction in obesity; thus, a fine balance between tissue remodeling and excessive accumulation of ECM proteins must be achieved to

maintain adipose tissue homeostasis (Sun et al., 2013). The direction of expression change in high-fat-fed SM/J mice reveals that their brown adipose expansion is associated with decreased expression of inflammatory (e.g., interleukin-7 receptor [*Il7r*]) (Kim et al., 2014) and fibrotic markers (e.g., collagen type VIII alpha 1 chain [*Col8a1*], semaphorin 3C [*Sema3c*]) (Mejhert et al., 2013; Sun et al., 2013), and changes in extracellular matrix components (e.g., matrix metallopeptidase 12 [*Mmp12*], procollagen c-endopeptidase enhancer [*Pcolce*]) (Huang et al., 2011; Lee et al., 2014) and cytokines (e.g., coagulation factor VII [*F7*], leptin [*Lep*], *Sfrp1*) (D'souza et al., 2017; Edén et al., 2015; Gauger et al., 2013) associated with metabolic health. Other mouse models of diet-induced obesity develop unhealthy brown adipose transcriptomes characterized by increased expression of pro-inflammatory genes and fibrotic markers (Alcalá et al., 2017). The direction of expression change in SM/J brown adipose tissue supports the uniqueness of this mouse model.

Increased Sfrp1 Expression in Expanded Brown Adipose Tissue Correlates with Improved Glucose Tolerance

We focused on *Sfrp1* as a candidate gene that may underlie the increased brown adipose mass in SM/J high-fat-fed mice. *Sfrp1* is a cytokine that inhibits Wnt/β-catenin signaling. Wnt/β-catenin signaling promotes the fibroblast identity, and *Sfrp1* blocks Wnt signaling to promote adipogenesis (Gauger et al., 2013; Lagathu et al., 2010; Wang et al., 2018). Its expression significantly increases in high-fat-fed SM/J brown adipose between 20 and 30 weeks, when the mice increase the size of their brown adipose depots and enter diabetic remission, and does not increase in white adipose of these same animals, or in the white or brown adipose of LG/J mice (Figures 4A and 4B; Figures S3A and S3B). Further, *Sfrp1* expression significantly correlates with brown adipose depot mass and with improved glucose tolerance in high-fat-fed SM/J mice (Figures 4C and 4D). We performed mediation analysis and found that the effects of *Sfrp1* expression on glucose tolerance in high-fat-fed SM/J mice is significantly mediated by brown adipose mass ($p = 0.004$). Data from a human genome-wide association study (GWAS) revealed several variants in the SFRP1 locus, including one variant (rs973441) that is significantly associated with type 2 diabetes adjusted for body mass index (BMI) (Figure 4E) (Mahajan et al., 2018). There are several variants in the *Sfrp1* locus between SM/J and LG/J genetic backgrounds, and the gene is located within the support intervals of QTL associated with adiposity and glucose tolerance that were mapped in an F_{16} LG × SM intercross (Figure 4F) (Lawson et al., 2010, 2011). These data further underscore that the SM/J genetic background has unique variants that contribute to its brown adipose expansion and diabetic remission. We hypothesize that DNA variants in SM/J mice increase *Sfrp1*, which in turn promotes brown adipogenesis by inhibiting Wnt/β-catenin signaling, and this in turn may contribute to the tissue's role as a glucose sink (Figure 4G).

DISCUSSION

Brown adipose has anti-diabetic properties that are conserved between mice and humans (Chechi et al., 2013; Cypess et al., 2009; Hanssen et al., 2016; van Marken Lichtenbelt et al., 2009; Saito, 2013; Saito et al., 2009; Stanford et al., 2013; Virtanen et al., 2009). Most brown adipose tissue research focuses on the effects of non-shivering thermogenesis on metabolic health. However, brown adipose coordinates a diverse array of physiological processes through the action of secreted factors associated with glucose homeostasis (e.g., fibroblast growth factor 21 [FGF21], bone morphogenic proteins [BMPs], Vascular endothelial growth factor A [VEGFA], interleukin 6 [IL-6], neuregulin 4 [NRG4]) (Poekes et al., 2015; Villarroya et al., 2017, 2019; Kajimura et al., 2015). Further, the mechanism of insulin-stimulated glucose uptake into brown adipose tissue was well established before the discovery of beta-adrenergic stimulation of thermogenesis (Marette and Bukowiecki, 1989). This mechanism is independent of UCP1 activity (Inokuma et al., 2005; Olsen et al., 2019; Orava et al., 2011). Insulin-stimulated glucose uptake increases in animals with brown adipose transplants (Stanford et al., 2013) and is blunted under obese (Orava et al., 2013) and diabetic conditions (Lapa et al., 2017). Here we report a natural expansion of brown adipose tissue in obese mice that coincides not with increased thermogenesis, but with improved insulin sensitivity, likely through increased insulin-stimulated glucose uptake into the brown adipose tissue. We have shown corresponding increased expression of two critical members of the insulin signaling pathway: *Glut4*, which mediates insulin-stimulated, but not norepinephrine-stimulated, glucose uptake (Shimizu et al., 1996), and *Irs1*, which is also necessary for brown adipose differentiation (Fasshauer et al., 2001). It is possible that brown adipose expansion in high-fat-fed SM/J mice is a protective mechanism to improve insulin sensitivity before the hyperglycemia gets out of control.

We found that genes associated with cytokine activity are enriched in the expanded tissue and diabetic remission. Cytokine secretion likely contributes to the obesity-independent ability of SM/J's brown adipose tissue to affect systemic glucose metabolism (Matsushita et al., 2014; Samms et al., 2015). We highlight *Sfrp1* as a particularly intriguing cytokine that may underlie this phenomenon. *Sfrp1* inhibits Wnt signaling, thus promoting adipogenesis (Ackers and Malgor, 2018; Bennett et al., 2002; Lagathu et al., 2010). Expression of *Sfrp1* increases as adipocytes differentiate, proportional to the strength of adipogenic stimulation, and also increases during treatment with thiazolidinedione drugs, which generally act through improving insulin-mediated glucose metabolism (Lagathu et al., 2009). Although *Sfrp1* has never been directly studied in brown adipose tissue, it is a member of a brown adipose coexpression module of genes enriched for cell division, with its expression strongly correlated with brown adipose mass in particular (Carson and Lawson, 2020).

In human obesity, *SFRP1* expression is downregulated in subcutaneous white adipose tissue, correlating with impaired insulin sensitivity (Ehrlund et al., 2013). Further, its expression was found to be deficient in obese patients with glycemic dysfunction (Chen and Wang, 2018; Ehrlund et al., 2013; Lagathu et al., 2010). Finally, high-fat-fed *Sfrp1*$^{-/-}$ mice show dysregulation of glucose metabolism, including downregulation of *Glut4* in white adipose tissue (Gauger et al., 2013). We show increased *Sfrp1* expression in an expanding brown adipose depot that corresponds with increased *Glut4* expression underlying potential

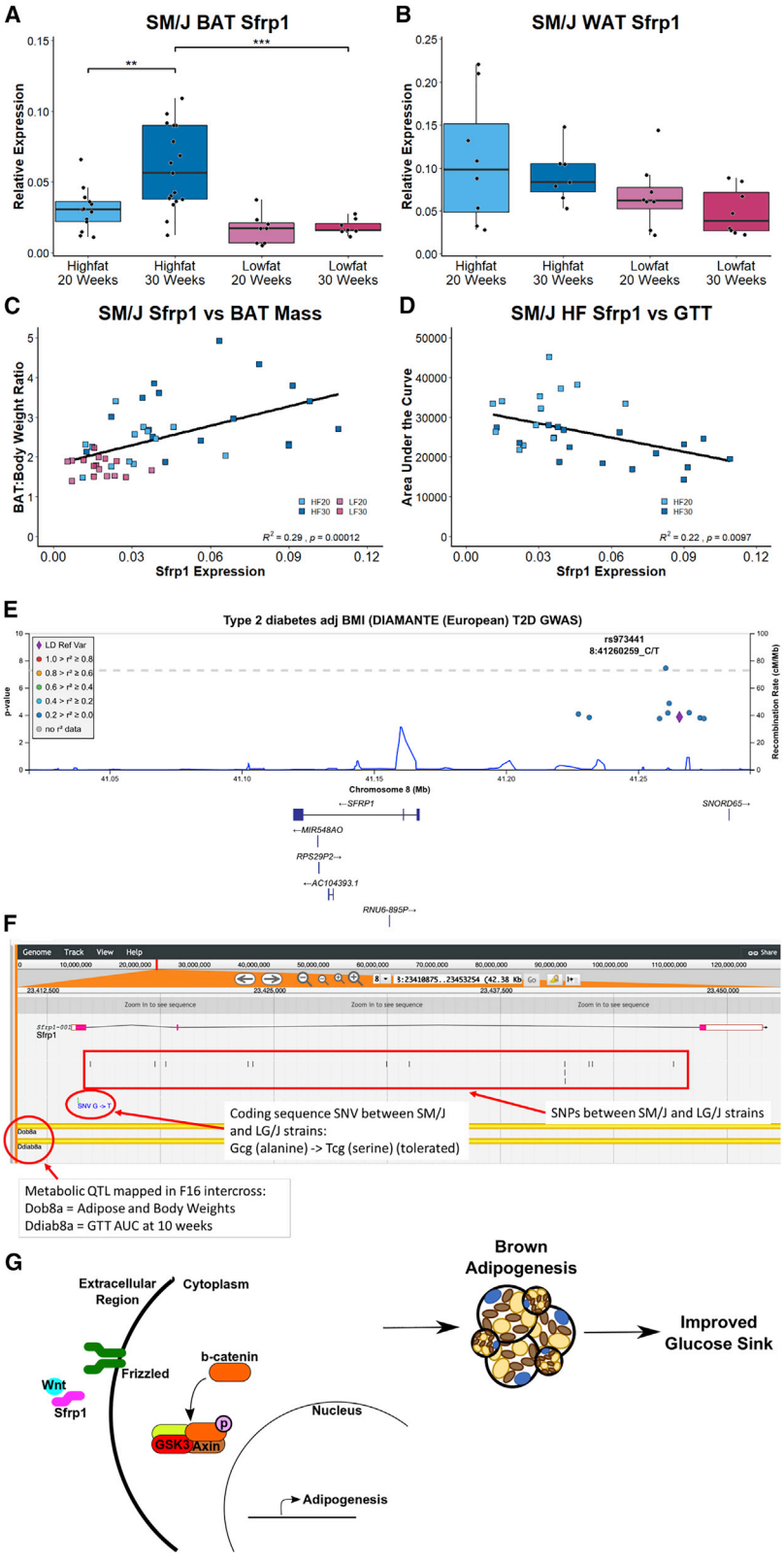

Figure 4. Increased Expression of *Sfrp1* Is Likely Culprit of Brown Adipose Tissue Expansion

(A and B) Expression of *Sfrp1* increases in (A) brown, but not (B) white, adipose tissue of high-fat-fed animals.

(C and D) *Sfrp1* expression correlates with brown adipose mass across cohorts (C) and with improved glucose tolerance in high-fat-fed SM/J mice (D).

(E) Screenshot of variants in human adipose tissue in the *SFRP1* locus region. Rs973441 is significantly linked with type 2 diabetes adjusted for BMI.

(F) The *Sfrp1* locus region contains multiple variants between SM/J and LG/J strains and is located in the quantitative trait locus (QTL) associated with adipose weight and glucose tolerance mapped in an F16 intercross of the strains.

(G) Model of Sfrp1 acting to increase brown adipogenesis. Sfrp1 sequesters Wnt away from its receptor, leading to phosphorylation and degradation of beta-catenin and thus allowing an adipogenic transcriptional program. The boxplots display median, 1st and 3rd quartiles, and 1.5 × interquartile range for each cohort. Individual data points are also represented. Equal numbers of males and females are represented; n = 8–17 mice per cohort. *p < 0.05, **p < 0.01, ***p < 0.001.

See also Figure S3.

improvement in insulin-stimulated glucose uptake. Although previous studies of *Sfrp1* have been conducted only in white adipose tissue, the data we present fit a model where brown adipocyte-secreted SFRP1 may act in an autocrine manner to stimulate brown adipose proliferation, leading to its role as an insulin-stimulated glucose sink and resulting in improved glucose tolerance and insulin sensitivity.

There is great interest in harnessing the potential of brown adipose to treat obesity and diabetes, either through the calorie-burning action of non-shivering thermogenesis or the endocrine action of adipokines. Research into the effects of brown adipose on systemic metabolism is in its infancy, and the community needs appropriate animal models to interrogate its physiological roles and identify potentially druggable targets. We present the SM/J mouse strain as a unique model to address this need. The SM/J mouse provides a tractable, genetic system in which to understand the relationship between brown adipose and glycemic control in obesity. Understanding this relationship in the SM/J mouse will open doors for identifying novel, potentially druggable targets for the improvement of glycemic control in humans.

STAR★METHODS

Detailed methods are provided in the online version of this paper and include the following:

- KEY RESOURCES TABLE
- RESOURCE AVAILABILITY
  - Lead Contact
  - Materials Availability
  - Data and Code Availability
- EXPERIMENTAL MODEL AND SUBJECT DETAILS
- METHOD DETAILS
  - Phenotyping
  - Blood plasma assays
  - Adipose histology
  - H&E Staining
  - Immunofluorescence
  - Quantitative rt-PCR
  - Mitochondrial DNA quantification
  - RNA sequencing and analyses
  - Brown adipose excision
- QUANTIFICATION AND STATISTICAL ANALYSIS

SUPPLEMENTAL INFORMATION

Supplemental Information can be found online at https://doi.org/10.1016/j.celrep.2020.108237.

ACKNOWLEDGMENTS

This work was supported by the Washington University Department of Genetics, the Diabetes Research Center at Washington University (grant P30DK020579), the NIH NIDDK (grant K01 DK095003 to H.A.L.), and NIH NIGM (grant T32 GM007067 to C.C.).

AUTHOR CONTRIBUTIONS

H.A.L. and C.C. designed the experiments. C.C., H.S., J.P.W., and H.A.L. performed physiological and molecular assays. C.C., M.A.M., and S.O. performed histological assays and analyses. C.C. and S.G. performed excision surgeries. C.C., J.F.M.-V., C.L.S.P., and H.A.L. analyzed the RNA-seq data. C.C. and H.A.L. wrote the manuscript. All authors edited and approved the final draft.

DECLARATION OF INTERESTS

The authors declare no competing interests.

Received: April 2, 2020
Revised: August 9, 2020
Accepted: September 15, 2020
Published: October 6, 2020

REFERENCES

Ackers, I., and Malgor, R. (2018). Interrelationship of canonical and non-canonical Wnt signalling pathways in chronic metabolic diseases. Diab. Vasc. Dis. Res. *15*, 3–13.

Alcalá, M., Calderon-Dominguez, M., Bustos, E., Ramos, P., Casals, N., Serra, D., Viana, M., and Herrero, L. (2017). Increased inflammation, oxidative stress and mitochondrial respiration in brown adipose tissue from obese mice. Sci. Rep. *7*, 16082.

Bennett, C.N., Ross, S.E., Longo, K.A., Bajnok, L., Hemati, N., Johnson, K.W., Harrison, S.D., and MacDougald, O.A. (2002). Regulation of Wnt signaling during adipogenesis. J. Biol. Chem. *277*, 30998–31004.

Carson, C., and Lawson, H.A. (2020). Genetic background and diet affect brown adipose gene coexpression networks associated with metabolic phenotypes. Physiol. Genomics *52*, 223–233.

Chechi, K., Carpentier, A.C., and Richard, D. (2013). Understanding the brown adipocyte as a contributor to energy homeostasis. Trends Endocrinol. Metab. *24*, 408–420.

Chen, Y., Lun, A.T.L., and Smythe, G.K. (2014). Differential expression analysis of complex RNAseq experiments using edgeR. Statistical Analysis of Next Generation Sequence Data (New York: Springer).

Chen, N., and Wang, J. (2018). Wnt/β-Catenin signaling and obesity. Front. Physiol. *9*, 792.

Cheverud, J.M., Lawson, H.A., Fawcett, G.L., Wang, B., Pletscher, L.S., Fox, A.R., Maxwell, T.J., Ehrich, T.H., Kenney-Hunt, J.P., Wolf, J.B., and Semenkovich, C.F. (2011). Diet-dependent genetic and genomic imprinting effects on obesity in mice. Obesity (Silver Spring) *19*, 160–170.

Chondronikola, M., Volpi, E., Børsheim, E., Porter, C., Annamalai, P., Enerbäck, S., Lidell, M.E., Saraf, M.K., Labbe, S.M., Hurren, N.M., et al. (2014). Brown adipose tissue improves whole-body glucose homeostasis and insulin sensitivity in humans. Diabetes *63*, 4089–4099.

Cypess, A.M., Lehman, S., Williams, G., Tal, I., Rodman, D., Goldfine, A.B., Kuo, F.C., Palmer, E.L., Tseng, Y.-H., Doria, A., et al. (2009). Identification and importance of brown adipose tissue in adult humans. N. Engl. J. Med. *360*, 1509–1517.

D'souza, A.M., Neumann, U.H., Glavas, M.M., and Kieffer, T.J. (2017). The glucoregulatory actions of leptin. Mol. Metab. *6*, 1052–1065.

Dobin, A., Davis, C.A., Schlesinger, F., Drenkow, J., Zaleski, C., Jha, S., Batut, P., Chaisson, M., and Gingeras, T.R. (2013). STAR: ultrafast universal RNA-seq aligner. Bioinformatics *29*, 15–21.

Edén, D., Siegbahn, A., and Mokhtari, D. (2015). Tissue factor/factor VIIa signalling promotes cytokine-induced beta cell death and impairs glucose-stimulated insulin secretion from human pancreatic islets. Diabetologia *58*, 2563–2572.

Ehrich, T.H., Kenney, J.P., Vaughn, T.T., Pletscher, L.S., and Cheverud, J.M. (2003). Diet, obesity, and hyperglycemia in LG/J and SM/J mice. Obes. Res. *11*, 1400–1410.

Ehrlund, A., Mejhert, N., Lorente-Cebrián, S., Aström, G., Dahlman, I., Laurencikiene, J., and Rydén, M. (2013). Characterization of the Wnt inhibitors secreted frizzled-related proteins (SFRPs) in human adipose tissue. J. Clin. Endocrinol. Metab. *98*, E503–E508.

Fasshauer, M., Klein, J., Kriauciunas, K.M., Ueki, K., Benito, M., and Kahn, C.R. (2001). Essential role of insulin receptor substrate 1 in differentiation of brown adipocytes. Mol. Cell. Biol. *21*, 319–329.

Gauger, K.J., Bassa, L.M., Henchey, E.M., Wyman, J., Bentley, B., Brown, M., Shimono, A., and Schneider, S.S. (2013). Mice deficient in Sfrp1 exhibit increased adiposity, dysregulated glucose metabolism, and enhanced macrophage infiltration. PLoS ONE *8*, e78320.

Goossens, G.H. (2017). The Metabolic Phenotype in Obesity: Fat Mass, Body Fat Distribution, and Adipose Tissue Function. Obes. Facts *10*, 207–215.

Gunawardana, S.C., and Piston, D.W. (2012). Reversal of type 1 diabetes in mice by brown adipose tissue transplant. Diabetes *61*, 674–682.

Hanssen, M.J.W., van der Lans, A.A.J.J., Brans, B., Hoeks, J., Jardon, K.M.C., Schaart, G., Mottaghy, F.M., Schrauwen, P., and van Marken Lichtenbelt, W.D. (2016). Short-term Cold Acclimation Recruits Brown Adipose Tissue in Obese Humans. Diabetes *65*, 1179–1189.

Huang, G., Ge, G., Wang, D., Gopalakrishnan, B., Butz, D.H., Colman, R.J., Nagy, A., and Greenspan, D.S. (2011). α3(V) Collagen is critical for glucose homeostasis in mice due to effects in pancreatic islets and peripheral tissues. J. Clin. Invest. *121*, 769–783.

Inokuma, K., Ogura-Okamatsu, Y., Toda, C., Kimura, K., Yamashita, H., and Saito, M. (2005). Uncoupling protein 1 is necessary for norepinephrine-induced glucose utilization in brown adipose tissue. Diabetes *54*, 1385–1391.

Kajimura, S., Spiegelman, B.M., and Seale, P. (2015). Brown and Beige Fat: Physiological Roles beyond Heat Generation. Cell Metab. *22*, 546–559.

Kim, D., Kim, J., Yoon, J.H., Ghim, J., Yea, K., Song, P., Park, S., Lee, A., Hong, C.P., Jang, M.S., et al. (2014). CXCL12 secreted from adipose tissue recruits macrophages and induces insulin resistance in mice. Diabetologia *57*, 1456–1465.

Klöting, N., Fasshauer, M., Dietrich, A., Kovacs, P., Schön, M.R., Kern, M., Stumvoll, M., and Blüher, M. (2010). Insulin-sensitive obesity. Am. J. Physiol. Endocrinol. Metab. *299*, E506–E515.

Lagathu, C., Christodoulides, C., Virtue, S., Cawthorn, W.P., Franzin, C., Kimber, W.A., Nora, E.D., Campbell, M., Medina-Gomez, G., Cheyette, B.N.R., et al. (2009). Dact1, a nutritionally regulated preadipocyte gene, controls adipogenesis by coordinating the Wnt/beta-catenin signaling network. Diabetes *58*, 609–619.

Lagathu, C., Christodoulides, C., Tan, C.Y., Virtue, S., Laudes, M., Campbell, M., Ishikawa, K., Ortega, F., Tinahones, F.J., Fernández-Real, J.M., et al. (2010). Secreted frizzled-related protein 1 regulates adipose tissue expansion and is dysregulated in severe obesity. Int. J. Obes. *34*, 1695–1705.

Lapa, C., Arias-Loza, P., Hayakawa, N., Wakabayashi, H., Werner, R.A., Chen, X., Shinaji, T., Herrmann, K., Pelzer, T., and Higuchi, T. (2017). Whitening and impaired glucose utilization of brown adipose tissue in a rat model of type 2 diabetes mellitus. Sci. Rep. *7*, 16795.

Lawson, H.A., Zelle, K.M., Fawcett, G.L., Wang, B., Pletscher, L.S., Maxwell, T.J., Ehrich, T.H., Kenney-Hunt, J.P., Wolf, J.B., Semenkovich, C.F., and Cheverud, J.M. (2010). Genetic, epigenetic, and gene-by-diet interaction effects underlie variation in serum lipids in a LG/JxSM/J murine model. J. Lipid Res. *51*, 2976–2984.

Lawson, H.A., Lee, A., Fawcett, G.L., Wang, B., Pletscher, L.S., Maxwell, T.J., Ehrich, T.H., Kenney-Hunt, J.P., Wolf, J.B., Semenkovich, C.F., and Cheverud, J.M. (2011). The importance of context to the genetic architecture of diabetes-related traits is revealed in a genome-wide scan of a LG/J × SM/J murine model. Mamm. Genome *22*, 197–208.

Lee, J.-T., Pamir, N., Liu, N.-C., Kirk, E.A., Averill, M.M., Becker, L., Larson, I., Hagman, D.K., Foster-Schubert, K.E., van Yserloo, B., et al. (2014). Macrophage metalloelastase (MMP12) regulates adipose tissue expansion, insulin sensitivity, and expression of inducible nitric oxide synthase. Endocrinology. *155*, 3409–3420.

Lin, J.Z., and Farmer, S.R. (2016). Morphogenetics in brown, beige and white fat development. Adipocyte *5*, 130–135.

Mahajan, A., Taliun, D., Thurner, M., Robertson, N.R., Torres, J.M., Rayner, N.W., Payne, A.J., Steinthorsdottir, V., Scott, R.A., Grarup, N., et al. (2018). Fine-mapping type 2 diabetes loci to single-variant resolution using high-density imputation and islet-specific epigenome maps. Nat. Genet. *50*, 1505–1513.

Marette, A., and Bukowiecki, L.J. (1989). Stimulation of glucose transport by insulin and norepinephrine in isolated rat brown adipocytes. Am. J. Physiol. *257*, C714–C721.

Matsushita, M., Yoneshiro, T., Aita, S., Kameya, T., Sugie, H., and Saito, M. (2014). Impact of brown adipose tissue on body fatness and glucose metabolism in healthy humans. Int. J. Obes. *38*, 812–817.

Meigs, J.B., Wilson, P.W.F., Fox, C.S., Vasan, R.S., Nathan, D.M., Sullivan, L.M., and D'Agostino, R.B. (2006). Body mass index, metabolic syndrome, and risk of type 2 diabetes or cardiovascular disease. J. Clin. Endocrinol. Metab. *91*, 2906–2912.

Mejhert, N., Wilfling, F., Esteve, D., Galitzky, J., Pellegrinelli, V., Kolditz, C.I., Viguerie, N., Tordjman, J., Näslund, E., Trayhurn, P., et al. (2013). Semaphorin 3C is a novel adipokine linked to extracellular matrix composition. Diabetologia *56*, 1792–1801.

Miranda, M.A., Carson, C., St Pierre, C.L., Macias-Velasco, J.F., Hughes, J.W., Schmidt, H., Wayhart, J.P., and Lawson, H.A. (2020). Spontaneous restoration of functional β-cell mass in obese SM/J mice. bioRxiv. https://doi.org/10.1101/2020.05.19.104588.

Nikolskiy, I., Conrad, D.F., Chun, S., Fay, J.C., Cheverud, J.M., and Lawson, H.A. (2015). Using whole-genome sequences of the LG/J and SM/J inbred mouse strains to prioritize quantitative trait genes and nucleotides. BMC Genomics *16*, 415.

Olsen, J.M., Åslund, A., Bokhari, M.H., Hutchinson, D.S., and Bengtsson, T. (2019). Acute β-adrenoceptor mediated glucose clearance in brown adipose tissue; a distinct pathway independent of functional insulin signaling. Mol. Metab. *30*, 240–249.

Orava, J., Nuutila, P., Lidell, M.E., Oikonen, V., Noponen, T., Viljanen, T., Scheinin, M., Taittonen, M., Niemi, T., Enerbäck, S., and Virtanen, K.A. (2011). Different metabolic responses of human brown adipose tissue to activation by cold and insulin. Cell Metab. *14*, 272–279.

Orava, J., Nuutila, P., Noponen, T., Parkkola, R., Viljanen, T., Enerbäck, S., Rissanen, A., Pietiläinen, K.H., and Virtanen, K.A. (2013). Blunted metabolic responses to cold and insulin stimulation in brown adipose tissue of obese humans. Obesity (Silver Spring) *21*, 2279–2287.

Pessin, J.E., and Saltiel, A.R. (2000). Signaling pathways in insulin action: molecular targets of insulin resistance. J. Clin. Invest. *106*, 165–169.

Poekes, L., Lanthier, N., and Leclercq, I.A. (2015). Brown adipose tissue: a potential target in the fight against obesity and the metabolic syndrome. Clin. Sci. (Lond.) *129*, 933–949.

Roberts-Toler, C., O'Neill, B.T., and Cypess, A.M. (2015). Diet-induced obesity causes insulin resistance in mouse brown adipose tissue. Obesity (Silver Spring) *23*, 1765–1770.

Saito, M. (2013). Brown adipose tissue as a regulator of energy expenditure and body fat in humans. Diabetes Metab. J. *37*, 22–29.

Saito, M., Okamatsu-Ogura, Y., Matsushita, M., Watanabe, K., Yoneshiro, T., Nio-Kobayashi, J., Iwanaga, T., Miyagawa, M., Kameya, T., Nakada, K., et al. (2009). High incidence of metabolically active brown adipose tissue in healthy adult humans: effects of cold exposure and adiposity. Diabetes *58*, 1526–1531.

Samms, R.J., Smith, D.P., Cheng, C.C., Antonellis, P.P., Perfield, J.W., 2nd, Kharitonenkov, A., Gimeno, R.E., and Adams, A.C. (2015). Discrete Aspects of FGF21 In Vivo Pharmacology Do Not Require UCP1. Cell Rep. *11*, 991–999.

Shimizu, I., and Walsh, K. (2015). The Whitening of Brown Fat and Its Implications for Weight Management in Obesity. Curr. Obes. Rep. *4*, 224–229.

Shimizu, Y., Kielar, D., Minokoshi, Y., and Shimazu, T. (1996). Noradrenaline increases glucose transport into brown adipocytes in culture by a mechanism different from that of insulin. Biochem. J. *314*, 485–490.

Shimizu, I., Aprahamian, T., Kikuchi, R., Shimizu, A., Papanicolaou, K.N., MacLauchlan, S., Maruyama, S., and Walsh, K. (2014). Vascular rarefaction mediates whitening of brown fat in obesity. J. Clin. Invest. *124*, 2099–2112.

Stanford, K.I., Middelbeek, R.J.W., Townsend, K.L., An, D., Nygaard, E.B., Hitchcox, K.M., Markan, K.R., Nakano, K., Hirshman, M.F., Tseng, Y.-H., and Goodyear, L.J. (2013). Brown adipose tissue regulates glucose homeostasis and insulin sensitivity. J. Clin. Invest. *123*, 215–223.

Sun, K., Tordjman, J., Clément, K., and Scherer, P.E. (2013). Fibrosis and adipose tissue dysfunction. Cell Metab. *18*, 470–477.

van Marken Lichtenbelt, W.D., Vanhommerig, J.W., Smulders, N.M., Drossaerts, J.M.A.F.L., Kemerink, G.J., Bouvy, N.D., Schrauwen, P., and Teule, G.J.J. (2009). Cold-activated brown adipose tissue in healthy men. N. Engl. J. Med. *360*, 1500–1508.

Villarroya, F., Cereijo, R., Villarroya, J., and Giralt, M. (2017). Brown adipose tissue as a secretory organ. Nat. Rev. Endocrinol. *13*, 26–35.

Villarroya, J., Cereijo, R., Gavaldà-Navarro, A., Peyrou, M., Giralt, M., and Villarroya, F. (2019). New insights into the secretory functions of brown adipose tissue. J. Endocrinol. *243*, R19–R27.

Virtanen, K.A., Lidell, M.E., Orava, J., Heglind, M., Westergren, R., Niemi, T., Taittonen, M., Laine, J., Savisto, N.-J., Enerbäck, S., and Nuutila, P. (2009). Functional brown adipose tissue in healthy adults. N. Engl. J. Med. *360*, 1518–1525.

Wang, G.X., Zhao, X.Y., and Lin, J.D. (2015). The brown fat secretome: metabolic functions beyond thermogenesis. Trends Endocrinol. Metab. *26*, 231–237.

Wang, L., Wang, Y., Meng, Y., Zhang, C., and Di, L. (2018). GSK3-activated STAT5 regulates expression of SFRPs to modulate adipogenesis. FASEB J. *32*, 4714–4726.

Winzell, M.S., and Ahrén, B. (2004). The high-fat diet-fed mouse: a model for studying mechanisms and treatment of impaired glucose tolerance and type 2 diabetes. Diabetes *53* (*Suppl 3*), S215–S219.

Wu, J., Boström, P., Sparks, L.M., Ye, L., Choi, J.H., Giang, A.H., Khandekar, M., Virtanen, K.A., Nuutila, P., Schaart, G., et al. (2012). Beige adipocytes are a distinct type of thermogenic fat cell in mouse and human. Cell *150*, 366–376.

Zhang, B., Kirov, S., and Snoddy, J. (2005). WebGestalt: an integrated system for exploring gene sets in various biological contexts. Nucleic Acids Res. *33*, W741–W748.

STAR★METHODS

KEY RESOURCES TABLE

REAGENT or RESOURCE	SOURCE	IDENTIFIER
Antibodies		
rabbit anti-Ucp1	Sigma	Cat#U6382; RRID: AB_261838
mouse anti-pHH3	Invitrogen	Cat#MA5-15220; RRID: AB_11008586
donkey anti-rabbit 488	Abcam	Cat#ab150061; RRID: AB_2571722
donkey anti-mouse 647	Abcam	Cat#ab150107
hematoxylin	Leica Surgipath	Cat#3801570
eosin	Leica Surgipath	Cat#3801616
Critical Commercial Assays		
Free Fatty Acids ELISA	Wako Life Sciences	Cat#995-34693
Leptin ELISA	Crystal Chem	Cat#90030; RRID AB_2722664
Adiponectin ELISA	Crystal Chem	Cat#80569
IGF1 ELISA	Crystal Chem	Cat#80574
Glucagon ELISA	Crystal Chem	Cat#81518; RRID AB_2811007
Deposited Data		
RNA-sequencing data for brown and white adipose tissue	https://www.ncbi.nlm.nih.gov/geo/query/acc.cgi?acc=GSE157569	GSE157569
Experimental Models: Organisms/Strains		
Mouse: SM/J	Jackson Laboratory	RRID:IMSR_JAX:000687
Mouse: LG/J	Jackson Laboratory	RRID:IMSR_JAX000675
Software and Algorithms		
STAR	Dobin et al., 2013	N/A
edgeR	Chen et al., 2014	N/A
WEBGestalt	Zhang et al., 2005	N/A
Other		
High Fat Diet: 42% kcal from fat	Teklad	TD88137
Low Fat Diet: 15% kcal from fat	Research Diets	D12284

RESOURCE AVAILABILITY

Lead Contact

CFurther information and requests for resources and reagents should be directed to and will be fulfilled by the Lead Contact, Heather A. Lawson, Ph.D. (email: lawson@wustl.edu).

Materials Availability

This study did not generate new unique reagents.

Data and Code Availability

RNA-sequencing data generated for this study have been deposited at the Gene Expression Omnibus GSE157569 (https://www.ncbi.nlm.nih.gov/geo/query/acc.cgi?acc=GSE157569).

EXPERIMENTAL MODEL AND SUBJECT DETAILS

SM/J (RRID:IMSR_JAX:000687) and LG/J (RRID:IMSR_JAX:000675) mice were obtained from The Jackson Laboratory (Bar Harbor, ME). Experimental animals were generated at the Washington University School of Medicine and all experiments were approved by the Institutional Animal Care and Use Committee in accordance with the National Institutes of Health guidelines for the care and use of laboratory animals. Pups were weaned at 3 weeks and reared in same-sex cages of 3-5 animals until necropsy. At weaning, mice were randomly placed on a high fat diet (42% kcal from fat; Teklad TD88137) or an isocaloric low fat diet (15% kcal from fat; Research

Diets D12284) (Table S1). Feeding was *ad libitum*. The animal facility operates on a 12 hour light/dark cycle with a constant ambient temperature of 21°C. All experiments were performed during the light phase. Mice of both sexes were used for all experiments. Age information for experimental animals can be found in each figure or table legend.

METHOD DETAILS

Phenotyping

Animals were weighed weekly until sacrifice. At 8, 18, 28, 38, and 48 weeks of age, animals were fasted for four hours (starting at 9am) before an intraperitoneal glucose tolerance test (starting at 1pm). At 19, 29, 39, and 49 weeks of age animals were subject to an intraperitoneal insulin tolerance test. At 10, 20, 30, 40, or 50 weeks of age, body composition was determined by MRI for SM/J mice. Body temperature of animals at 20 and 30 weeks of age was determined using a rectal thermometer. All animals were fasted for four hours, then given an overdose of sodium pentobarbital. Once the animals were anesthetized, blood was collected via cardiac puncture and euthanasia was achieved by cardiac perfusion with phosphate-buffered saline. After cardiac perfusion, tissues were collected and flash frozen in liquid nitrogen and stored at −80°C, or processed according to protocols for histology and other assays.

Blood plasma assays

Fasting blood glucose was measured using a GLUCOCARD Vital glucometer (Arkay, MN USA). ELISAs measuring plasma levels of free fatty acids (Wako Life Sciences 995-34693), leptin (Crystal Chem #90030), adiponectin (Crystal Chem #80569), IGF1 (Crystal Chem #80574), and glucagon (Crystal Chem #81518) were quantified according to manufacturer's protocol. Catecholamines were assayed through the Vanderbilt University Medical Center's Hormone Assay and Analytical Services Core (https://www.vumc.org/hormone/assays; NIH grants DK059637 (MMPC) and DK020593 (DRTC)).

Adipose histology

At the time of tissue collection, small portions of interscapular brown and reproductive white adipose tissues were placed in 1 mL of neutral buffered formalin. These samples were incubated at 4°C while gently shaking for 24 hours. Immediately afterward, samples were placed into plastic cages and processed into paraffin blocks using a Leica tissue processor with the following protocol: 70% EtOH for 1 hour x 2, 85% EtOH for 1 hour, 95% EtOH for 1 hour x 2, 100% EtOH for 1 hour x 2, Xylenes for 1 hour x 2, paraffin wax. Adipose blocks were sectioned into 6 μm sections, with 2-4 slices on each slide.

H&E Staining

Slides were incubated at 60°C for 1 hour, then placed in xylenes to remove remaining paraffin wax. Slides were then rehydrated using successive decreasing EtOH concentrations (xylenes x 2, 100% EtOH x 2, 95% EtOH, 70% EtOH, H2O). Slides were incubated in hematoxylin (Leica Surgipath 3801570), Define (3803590), Blue Buffer 8 (3802915), and eosin (3801616), and dehydrated (95% EtOH, 100% EtOH, xylene x 2). Imaging was performed using the Zeiss AxioPlan2 microscope and Olympus DP software. Analysis of adipocyte size was performed using ImageJ. Images were converted to black and white and skeletonized to reveal only the cell wall outlines. Cell area was calculated from outlines with a lower limit of 50 um and upper limit of 700 um to reduce noise. All cells from a cohort (4-7 images each from 4 animals per cohort, equal numbers of males and females) were pooled for cell area density analysis.

Immunofluorescence

Slides were incubated at 60°C for 1 hour, then placed in xylenes to remove remaining paraffin wax. Slides were then rehydrated using successive decreasing EtOH concentrations (xylenes x 2, 50% EtOH in xylenes, 100% EtOH x 2, 95% EtOH, 70% EtOH, 50% EtOH, 0.3% H2O2 in MeOH, H2O). Slides were washed with TBS and blocked in 10% normal donkey serum (Abcam ab7475) for 1 hour, followed by incubation with primary antibody overnight at 4°C. [Primary antibodies: rabbit anti-Ucp1 (1:100, Sigma U6382) and mouse anti-PHH3 (1:100, Invitrogen MA5-15220)]. After an additional wash, secondary antibody was applied for 1 hour at room temperature [Secondary antibodies: donkey anti-rabbit 488 (1:1000, Abcam ab150061) and donkey anti-mouse 647 (1:200, Abcam ab150107)]. Fluoroshield Mounting Medium with DAPI (Abcam) was applied to seal the coverslip and slides were stored at 4°C. Imaging was performed using the Zeiss Confocal microscope and Zen Lite imaging program. PHH3 analysis was performed using the CellProfiler program. Background was subtracted from DAPI and PHH3 channels using ImageJ. DAPI channel was used to identify total nuclei in CellProfiler. Adipose nuclei images were overlaid with PHH3 stain to identify mitotic adipose nuclei. Mitotic nuclei were summed across all 4 slides for each individual. Mitotic adipose index is reported as mitotic adipose nuclei divided by adipose nuclei multiplied by 100%.

Quantitative rt-PCR

Total RNA was extracted from brown, subcutaneous inguinal, and visceral reproductive adipose samples using the QIAGEN RNeasy Lipid Kit. High-Capacity cDNA Reverse Transcription Kit (Thermofisher) was used for reverse transcription. Quantitative-rtPCR was performed to assess expression levels of target genes with an Applied Biosystems (USA) QuantStudio 6 Flex instrument using SYBR Green reagent. Results were normalized to *L32* expression, which was experimentally determined to not be differentially expressed across diet and age cohorts. cDNA products were analyzed by the ΔC_T method. Primers: *L32* forward TCCACAATGTCAAGG

AGCTG, reverse GGGATTGGTGACTCTGATGG; *Adipoq* forward ACGTCATCTTCGGCATGACT, reverse CTCTAAAGATTGTCA GTCCATCTG ; *Cidea* forward TGCTCTTCTGTATCGCCCAGT, reverse GCCGTGTTAAGGAATCTGCTG; *Eva1* forward CCACTTCTCCTGAGTTTACAGC reverse GCATTTTAACCGAACATCTGTCC; *Fabp4* forward CACTTTCCTTGTGGCAAAGC, reverse AATGTGTGATGCCTTTGTGG ; *Pparg* forward GAATGCGAGTGGTCTTCCAT, reverse TGCACTGCCTATGAGCACTT; *Prdm16* forward CCACCAGCGAGGACTTCAC reverse GGAGGACTCTCGTAGCTCGAA; *Sfrp1* forward TACTGGCCCGAGATGCTCAA, reverse GAGGCTTCCGTGGTATTGGG; *Tbx1* forward GGCAGGCAGACGAATGTTC, reverse TTGTCATCTACGGGCACAAAG; *Ucp1* forward CCTCTCCAGTGGATGTGGTAA, reverse AGAAGCCACAAACCCTTTGA.

Mitochondrial DNA quantification

DNA was extracted from brown and inguinal adipose tissues using the QIAGEN DNeasy Blood and Tissue Kit. Briefly, 40mg of tissue was homogenized in 10% proteinase K through vortexing and incubation at 56°C. DNA was precipitated with ethanol, collected in a spin column, and eluted in 150mL of buffer. DNA concentration was quantified on a Nanodrop, and 50ng was used in a qPCR reaction to quantify the amount of *h19* (nuclear gene) and *CytB* (mitochondrial gene). Mitochondrial content was calculated as the ratio of mtDNA to nucDNA. Primers used: *Cytb* forward TCTACGCTCAATCCCCAATAAAC, reverse TTAGGCTTCGTTGCTTTGAGGT; *h19* forward TATGTGCCATTCTGCTGCGA, reverse AAGGTTTAGAGAGGGGGCCT.

RNA sequencing and analyses

Sixty-four LG/J and SM/J mice were used for sequencing analysis, representing 4 males and 4 females from each diet (high and low fat) and age (20 and 30 weeks). Total RNA was isolated from interscapular brown and reproductive white adipose tissues using the RNeasy Lipid Tissue Kit (QIAgen). RNA concentration was measured via Nanodrop and RNA quality/integrity was assessed with a BioAnalyzer (Agilent). RNaseq libraries were constructed using the RiboZero kit (Illumina) from total RNA samples with RIN scores > 7.5. Libraries were checked for quality and concentration using the DNA 1000LabChip assay (Agilent) and quantitative PCR, according to manufacturer's protocol. Libraries were sequenced at 2x100 paired end reads on an Illumina HiSeq 4000. After sequencing, reads were de-multiplexed and assigned to individual samples.

FASTQ files were filtered to remove low quality reads and aligned against LG/J and SM/J custom genomes using STAR (Dobin et al., 2013; Nikolskiy et al., 2015). Briefly, LG/J and SM/J indels and SNVs were leveraged to construct strain-specific genomes using the GRC38.72-mm10 reference as a template. This was done by replacing reference bases with alternative LG/J and SM/J bases using custom python scripts. Ensembl R72 annotations were adjusted for indel-induced indexing differences for both genomes. Read counts were normalized via upper quartile normalization and a minimum normalized read depth of 10 was required. Alignment summaries are provided in Figure S4. Library complexity was assessed and differential expression between each age cohort for each strain-by-diet comparison was determined after TMM normalization in edgeR (Chen et al., 2014).

Functional enrichment of differentially expressed genes was tested by over-representation analysis in the WEB-based Gene Set Analysis Toolkit v2019 (Zhang et al., 2005). We performed analyses of gene ontologies (biological process, cellular component, molecular function), pathway (KEGG), and phenotype (Mammalian Phenotype Ontology). For each tissue, the list of all unique differentially expressed genes was analyzed against the background of all unique genes expressed in that tissue (Tables S2 and S3). A Benjamini-Hochberg FDR-corrected p value $\leq$ 0.05 was considered significant.

Brown adipose excision

Interscapular brown adipose tissue depots were removed from 20 or 30 week-old high fat-fed SM/J mice. A small longitudinal incision was made between the shoulder blades. All interscapular adipose tissue was carefully removed, and a cauterizing wand used to stop excessive bleeding when necessary. Surgeries were performed under general anesthesia by IP injection of ketamine/xylazine (100/200 mg/Kg) and mice were maintained in the surgical plane by isofluorane/oxygen for the duration of the procedure. Incisions were closed with 5-0 nonabsorbable sutures. Ketoprofen (2 mg/Kg) was provided post-procedure and topical antibiotic was applied to the incision daily for 3 days. Animal health and well-being was monitored daily. Sutures were removed at 10 days post-surgery. Mice were allowed to recover for four weeks after surgery or until they reached 30 weeks of age, then underwent a glucose tolerance test and an insulin tolerance test one week later. After an additional week of recovery, animals were sacrificed and plasma and multiple tissues harvested (reproductive and inguinal adipose depots, liver, heart, soleus, pancreas, hypothalamus) as described above.

QUANTIFICATION AND STATISTICAL ANALYSIS

Data within individual cohorts were assessed for normality using a Wilks-Shapiro test. Outliers were identified by a Grubbs test ($p < 0.05$) and removed. The sex X diet X age term was not significant for any phenotype so males and females were pooled for analyses. For all box-plots, data were tested for significant differences among cohorts by ANOVA with a Tukey's post hoc correction. A Welch's unequal variances t test was performed between ages in each diet to determine significant differences in adipocyte cell size distribution. Mediation analysis was performed using the 'mediation' package in R. P values < 0.05 were considered significant. All statistical analyses were performed using the R software package.

Cell Reports, Volume *33*

Supplemental Information

Brown Adipose Expansion and Remission of Glycemic Dysfunction in Obese SM/J Mice

Caryn Carson, Juan F. Macias-Velasco, Subhadra Gunawardana, Mario A. Miranda, Sakura Oyama, Celine L. St. Pierre, Heather Schmidt, Jessica P. Wayhart, and Heather A. Lawson

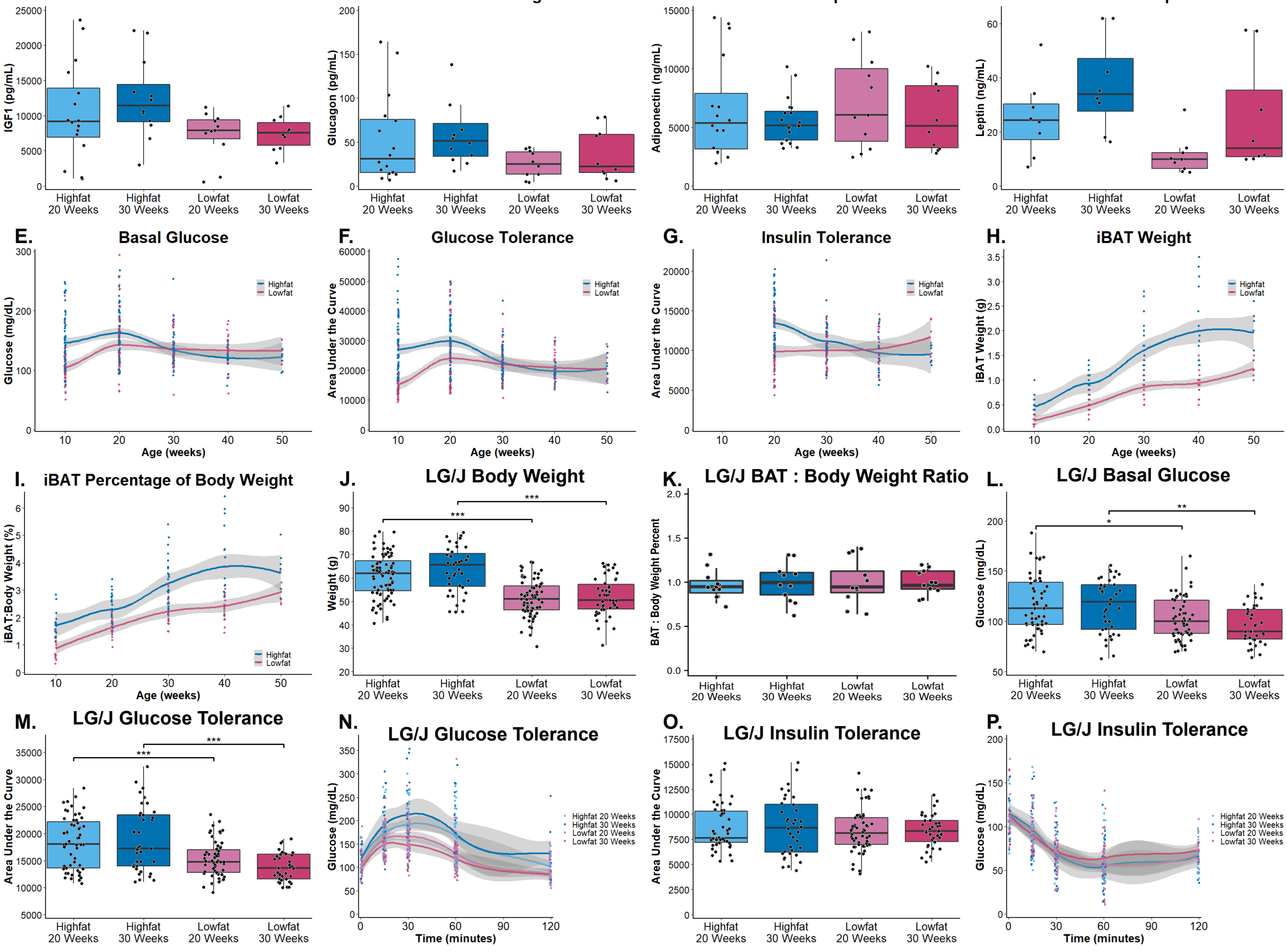

Figure S1: Physiological characterization of SM/J and LG/J mice (Related to Figure 1).

Plasma levels of IGF1 (**A**), glucagon (**B**), adiponectin (**C**), and leptin (**D**) in high and low fat-fed SM/J mice at 20 and 30 weeks. Basal glucose (**E**) and glucose tolerance (**F**) of high and low fat-fed SM/J mice at 10, 20, 30, 40, and 50 weeks. Insulin tolerance (**G**) of high and low fat-fed SM/J mice at 20, 30, 40, and 50 weeks. Interscapular brown adipose depot weight in grams (**H**) and as a percentage of total body weight (**I**) of SM/J mice at 10, 20, 30, 40, and 50 weeks. Body weight (**J**) and brown adipose tissue as a proportion of total body weight (**K**) in high and low fat-fed LG/J mice at 20 and 30 weeks of age. Basal glucose (**L**) and glucose tolerance (**M-N**) of high fat-fed LG/J mice are higher than low fat-fed controls at 30 weeks. Insulin sensitivity (**O-P**) is not different among the LG/J cohorts. The boxplots display median, 1st and 3rd quartiles, and 1.5*Interquartile Range for each cohort. Individual data points are also represented. Number of animals per cohort = 8-16 for panels **A-D**, 21-73 for panels **E-G**, 16-25 for panels **H-I**, and 30-60 for panels **J-P**. Approximately equal numbers of males and females represented. Statistical differences calculated among all cohorts using one-way ANOVA with Tukey's post hoc correction. *p<0.05, **p<0.01, ***p<0.0001

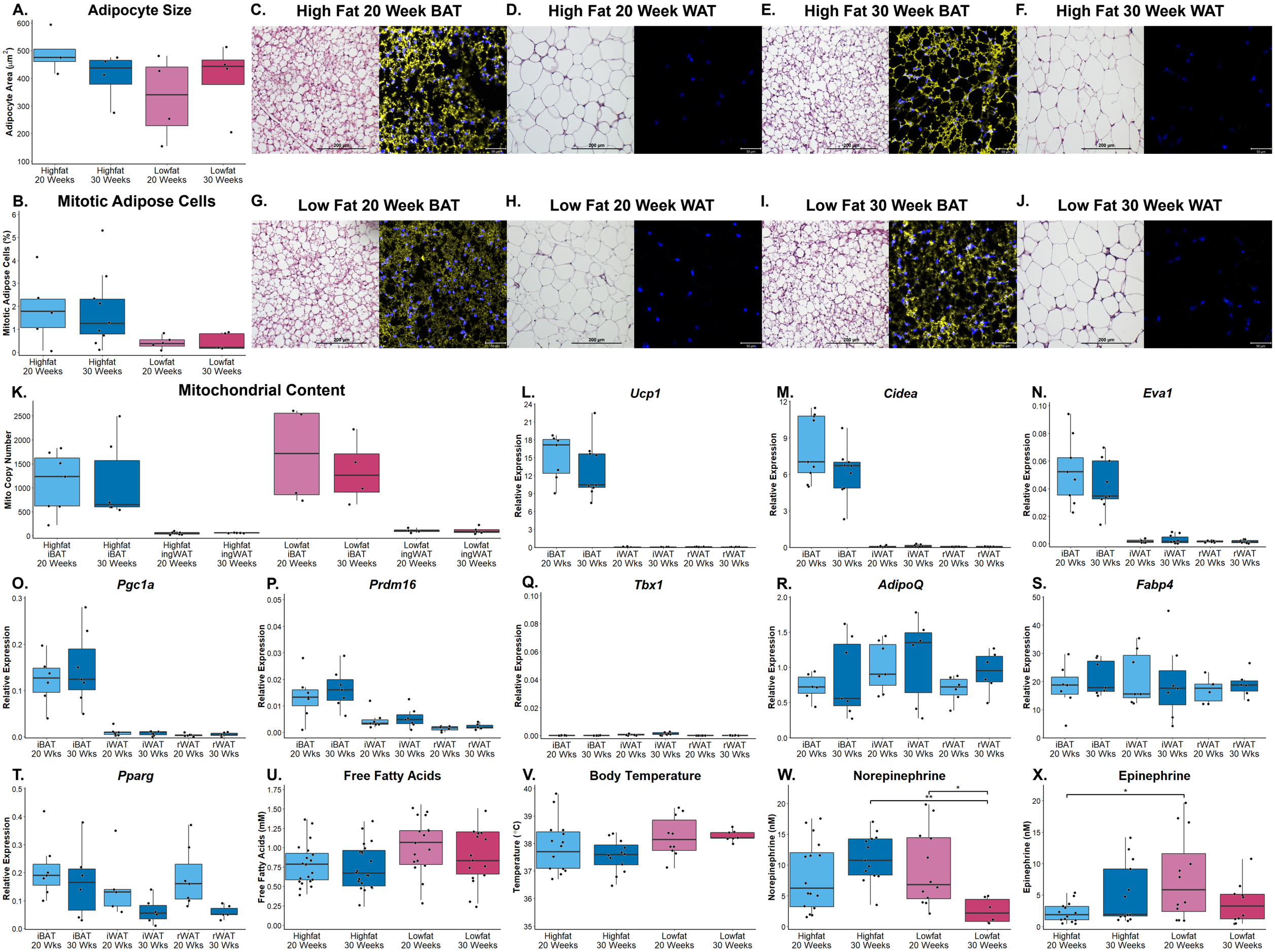

Figure S2: Morphology and thermogenic characteristics of SM/J brown adipose tissue (Related to Figure 2)

Quantification of average cell size (**A**) and percentage of phosphohistone H3 positive cells (**B**) in brown adipose depots of high and low fat-fed SM/J mice. Representative images of brown and white adipose from high fat-fed mice at 20 (**C-D**) and 30 weeks of age (**E-F**) and from low fat-fed mice at 20 (**G-H**) and 30 weeks of age (**I-J**). Stained for H&E (left picture, scale bar = 200nm) or UCP1 (yellow) and DAPI (blue) (right picture, scale bar = 50nm). Mitochondrial copy number (**K**) was significantly higher in brown adipose tissue than in inguinal white adipose tissue at both 20 and 30 week time points with no significant difference between high or low fat-fed mice. Gene expression levels (**L-T**) quantified in three adipose depots of high fat-fed mice: intrascapular brown adipose (iBAT), inguinal white adipose (ingWAT), and reproductive white adipose (repWAT). Canonical brown adipose genes Ucp1 (**L**), Cidea (**M**), Eva1 (**N**), Pgc1a (**O**), and Prdm16 (**P**) show high expression in iBAT and no difference between 20 and 30 week-old mice. Beige adipose marker Tbx1 (**Q**) is not expressed in any depot. All adipose depots had roughly equal expression of general adipose markers Adipoq (**R**), Fabp4/AP2 (**S**), and Pparg (**T**). Body temperature (U) and plasma free fatty acid (V), norepinephrine (W) and epinephrine (X) concentrations at time of necropsy. The boxplots display median, 1st and 3rd quartiles, and 1.5*Interquartile Range for each cohort. Individual data points are also represented. Number of animals per cohort = 4 for panels **A-B**, 6-10 for panels **K-T**, and 8-21 for panels **U-X**. Approximately equal numbers of males and females represented. Statistical differences calculated using one-way ANOVA with Tukey's post hoc correction among all cohorts in panels **A-B** and **U-X** and between 20 and 30 week cohorts within individual adipose depots for panels **K-T**. *p<0.05, **p<0.01, ***p<0.0001

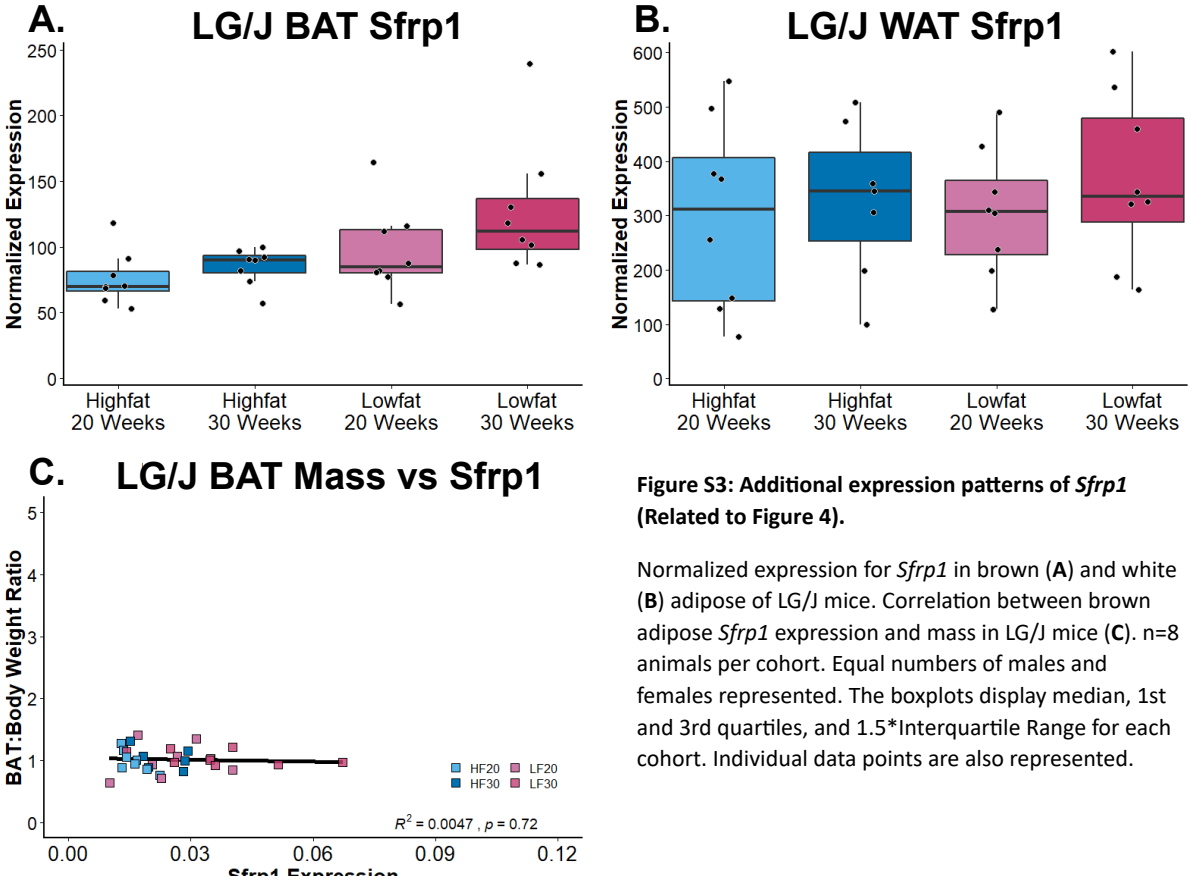

Figure S3: Additional expression patterns of *Sfrp1* (Related to Figure 4).

Normalized expression for *Sfrp1* in brown (**A**) and white (**B**) adipose of LG/J mice. Correlation between brown adipose *Sfrp1* expression and mass in LG/J mice (**C**). n=8 animals per cohort. Equal numbers of males and females represented. The boxplots display median, 1st and 3rd quartiles, and 1.5*Interquartile Range for each cohort. Individual data points are also represented.

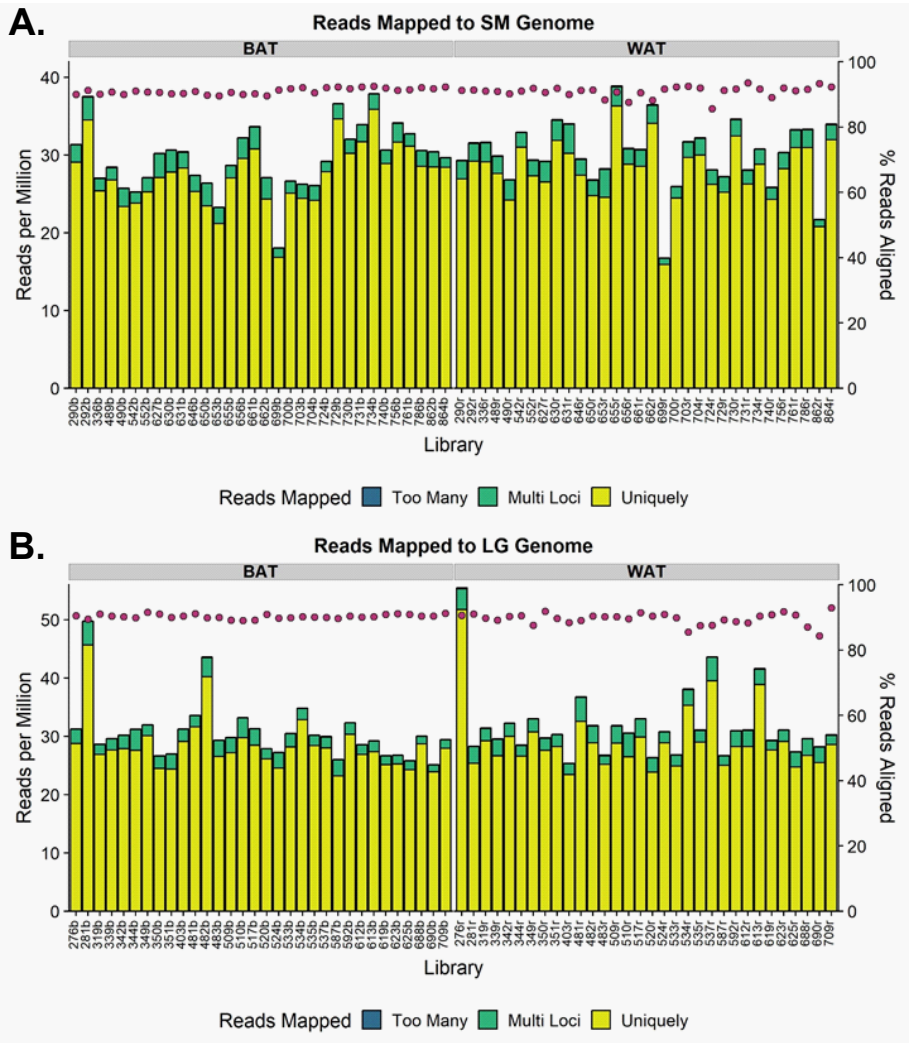

Figure S4: STAR alignment summaries for RNA-sequencing results (Related to STAR Methods)

Alignment summaries for RNA-sequencing results from (**A**) SM/J and (**B**) LG/J samples. Brown adipose samples are on the left, white adipose are on the right. Reads per million (left y-axis) are indicated by bars (yellow = uniquely mapped, green = multi loci, blue = mapped to too many loci) and % reads aligned (right x-axis) are indicated by red circles.

Table S1. High and low fat diet constituents

Source	High Fat[#]	Low Fat[*]
Energy from Fat	42%	15%
Casein (g/kg)	195	197
Sugars (g/kg)	341	307
Corn starch (g/kg)	150	313
Cellulose (g/kg)	50	30
Corn oil (g/kg)	---	58
Hydrogenated coconut oil (g/kg)	---	7
Anhydrous milkfat (g/kg)	210	---
Cholesterol (g/kg)	1.5	---
Total energy (kJ/g)	18.95	16.99

[#] Teklad TD88137

[*] Research Diets D12284

Table S1: High and low fat diet constituents (Related to STAR Methods). The diets (high fat: Teklad TD88137; low fat: Research Diets D12284) have been used in multiple studies of diet-induced obesity using the SM/J strain.